Estimates of free-tropospheric NO_2 and HCHO mixing ratios derived from high-altitude mountain MAX-DOAS observations in the mid-latitudes and tropics

S. F. Schreier, A. Richter, F. Wittrock, and J. P. Burrows

Institute of Environmental Physics, University of Bremen, Germany

Correspondence to: S. F. Schreier (schreier@iup.physik.uni-bremen.de)

Abstract

In this study, mixing ratios of NO_2 (X_{NO2}) and HCHO (X_{HCHO}) in the free troposphere are derived from two Multi-AXis Differential Optical Absorption Spectroscopy (MAX-DOAS) data sets collected at Zugspitze (2650 m a.s.l., Germany) and Pico Espejo (4765 m a.s.l., Venezuela). The estimation of NO_2 and HCHO mixing ratios is based on the modified geometrical approach, which assumes a single-scattering geometry and a scattering point altitude close to the instrument altitude. Firstly, the horizontal optical path length (hOPL) is obtained from O_4 differential slant column densities (DSCDs) in the horizontal (0°) and vertical (90°) viewing directions. Secondly, X_{NO2} and X_{HCHO} are estimated from the NO_2 and HCHO DSCDs at the 0° and 90° viewing directions and averaged along the obtained hOPLs. As the MAX-DOAS instrument was performing measurements in the ultraviolet region, wavelength ranges of 346-372 nm and 338-357 nm are selected for the DOAS analysis to retrieve NO_2 and HCHO DSCDs, respectively. In order to compare the measured O_4 DSCDs and moreover to perform some sensitivity tests, the radiative transfer model SCIATRAN with adapted altitude settings for mountainous terrain is operated to simulate synthetic spectra, on which the DOAS analysis is also applied. The overall agreement between measured and synthetic O_4 DSCDs is better for the higher Pico Espejo station than for Zugspitze. Further sensitivity analysis shows that a change in surface albedo (from 0.05 to 0.7) can influence the O_4 DSCDs, with a larger absolute difference observed for the horizontal viewing direction. Consequently, the hOPL can vary by about 5% throughout the season, for example when winter snow cover fully disappears in summer. Typical values of hOPLs during

clear sky conditions are 19 km (14 km) at Zugspitze and 34 km (26.5 km) at Pico Espejo when using the 346-372 nm (338-357 nm) fitting window. The estimated monthly values of X_{NO2} (X_{HCHO}), averaged over these hOPLs during clear sky conditions, are in the range of 60-100 ppt (500-950 ppt) at Zugspitze and 8.5-15.5 ppt (255-385 ppt) at Pico Espejo. Interestingly, multi-year averaged monthly means of X_{NO2} and X_{HCHO} increase towards the end of the dry season at the Pico Espejo site, suggesting that both trace gases are frequently lifted above the boundary layer as a result of South American biomass burning.

1 Introduction

Tropospheric nitrogen oxides ($NO_x = NO + NO_2$) are released from various human activities (e.g. the burning of oil, coal, gas, and wood). Natural sources of NO_x include lightning, wildfires, and microbial activity in soils (Lee et al., 1997). Nitric oxide (NO) is the predominant part of NO_x released from these sources, but it is quickly converted to nitrogen dioxide (NO_2) by reaction with ozone (O_3). The major part of NO_x emissions remains in the boundary layer (BL). However, in addition to NO_x from lightning, significant amounts of NO_x from surface sources occasionally reach the free troposphere (FT) due to meteorology, orographic uplift of BL air masses or pyro-convection.

Formaldehyde (HCHO) is the most abundant carbonyl in the atmosphere and a valuable tracer of volatile organic compound (VOC) sources as it is produced from the oxidation of VOCs. Major sources of HCHO include the oxidation of methane (CH_4) (Lowe and Schmidt, 1983) and non-methane hydrocarbons (NMHC) (Fried et al., 2003). While HCHO formation in the remote marine atmosphere is dominated by CH_4 oxidation (Weller et al., 2000), the major precursor of HCHO in the continental BL is isoprene (Guenther et al., 2006). Further sources of HCHO are direct emissions from biomass burning (Andreae and Merlet, 2001), anthropogenic combustion processes (Anderson et al., 1994), and vegetation (Seco et al., 2007).

As NO_2 and HCHO are good indicators of tropospheric pollution, extensive ground-based measurement networks have been exploited in order to monitor their amounts and distributions (WMO, 2010). While ground-based in situ measurements represent rather surface and/or local

amounts of NO_2 and HCHO, remote sensing techniques such as the Multi-AXis Differential Optical Absorption Spectroscopy (MAX-DOAS) have the potential to derive both horizontal and vertical distributions of these trace gases in the immediate vicinity of the station (Hönninger et al., 2004; Wittrock et al., 2004). There exist some records of NO_2 in the free troposphere from aircraft in situ measurements (Singh et al., 2009), and balloon-borne soundings (Kritten et al., 2010). However, these observations are sparse and mainly performed during short field campaigns. Recently, global free-tropospheric NO_2 mixing ratios have been obtained from satellite data using the cloud-slicing technique (Choi et al., 2014). While the overall order of magnitude of satellite-derived values is similar to those taken from aircraft in situ measurements, the agreement of individual comparisons is not always good. Data records of HCHO in the free troposphere are also rare and deduced at different seasons, regions, and altitudes (Schuster et al., 1990; Arlander et al., 1995; Singh et al., 2001).

Although the number of ground-based in situ and remote sensing instruments to observe tropospheric pollution has increased during the last years, the level of knowledge concerning representative NO_2 and HCHO amounts in the FT is still rather low up to now. There are two reasons for this: Firstly, ground-based in situ measurements performed at high altitude sites are influenced by air masses that are lifted along the mountain slope to the station (Reidmiller et al., 2010) and thus, often represent rather (polluted) BL air. Secondly, MAX-DOAS measurements have been mainly focused on the BL, where the vast majority of tropospheric pollution is found.

Only very recently, a novel approach to estimate NO_2 mixing ratios in the FT from MAX-DOAS measurements was proposed (Gomez et al., 2014). In that study, the retrieval of O_4 and NO_2 differential slant column densities (DSCDs) was performed in the visible part of the electromagnetic spectrum on the basis of data from nine summer days in Izaña having low aerosol levels. The MAX-DOAS observations of that study were performed at a high-altitude site in the subtropics. The great advantage of the method by Gomez et al. (2014) is to average trace gas concentrations over a long horizontal path (in the order of a few tens of kilometers) and thus, minimize local effects of BL air masses that are lifted to the station. A follow-up study to investigate the seasonal evolution of NO_2 in the free troposphere at the Izaña site was carried out by Gil-Ojeda et al. (2015). That study reported background NO_2 mixing ratios in the range of 20-45 ppt, with lowest (highest) NO_2 amounts in winter (summer).

The aim of the present study is to extend these two studies and provide estimates of NO_2 and HCHO mixing ratios in the FT. For this purpose, two long-term MAX-DOAS data sets from two high-altitude sites located in the mid-latitudes and tropics are analyzed. In contrast to Gomez et al. (2014) and Gil-Ojeda et al. (2015), the retrieval of O_4, NO_2, and HCHO DSCDs in our study is performed in the ultraviolet range of the electromagnetic spectrum. Here, we obtain monthly means of NO_2 and HCHO mixing ratios during clear sky conditions at the two measurement sites, focus on the seasonal variability, and compare our values with values reported in the literature. To the best of the authors' knowledge, this is the first study presenting HCHO mixing ratios in the FT based on long-term MAX-DOAS measurements.

In the following Sect. 2, the MAX-DOAS system and the two measurement locations are described. The modified geometrical approach as proposed by Gomez et al. (2014) to estimate horizontal optical path lengths (hOPLs) and mixing ratios of NO_2 from MAX-DOAS DSCDs is briefly summarized in Sect. 3. The simulation of synthetic spectra using the radiative transfer model SCIATRAN is described in Sect. 4. Details about the analysis of measured and synthetic spectra using the DOAS method are given in Sect. 5. The results of this study, including a comparison of measured and synthetic O_4 DSCDs and the analysis of hOPLs, NO_2 and HCHO mixing ratios for both locations, are presented in Sect. 6. A short summary and conclusions are given in Sect. 7.

2 Instrumentation and location

The MAX-DOAS system, which was operated at the two high altitude stations Zugspitze, Germany (47.5°N, 11°E, 2650 m a.s.l.) and Pico Espejo, Venezuela (8.5°N, 71°W, 4765 m a.s.l.), comprised a temperature stabilized grating spectrometer equipped with a cooled CCD detector. The spectrometer and CCD detector were housed inside a building and connected to a telescope unit, which was mounted outdoors. In addition to the zenith window, a horizon (off-axis) window was implemented in the telescope to allow for the scanning of different off-axis directions, which were controlled by a motorized mirror. Scattered sunlight entering the telescope, either from the zenith or horizon window, is focused by a lens to reduce the field of view before it reaches the optical fibre mount. During the instrument's operation at the two measurement stations, a field of

view with an opening angle of ~1° was achieved (Oetjen, 2009 and Peters, 2013). Consequently, the signal in the horizontal path might be slightly affected by the contribution of trace gas absorption at lower altitudes (up to 500 m below the measurement stations at the end of the hOPL). Nevertheless, the mixing ratios as presented in Sects. 6.3 and 6.4 for NO_2 and HCHO, respectively, are still considered to be representative for the free troposphere. As a result of the wavelength range of the spectrometer covering 321 to 410 nm, HCHO retrieval is possible and the retrieval of O_4 and NO_2 DSCDs is restricted to the UV spectral region in this study (see Sect. 5).

In February 2003, the MAX-DOAS instrument was temporarily set up at the mid-latitude site Zugspitze, Germany, where it performed measurements until the end of July 2003. The underlying intention behind choosing Zugspitze as a measurement location was the fact that MAX-DOAS measurements of NO_2 could be used to validate satellite-derived stratospheric NO_2 columns as most of the NO_2 above this altitude is assumed to belong to the stratosphere. The telescope was orientated at 120° azimuth (east-southeast) throughout the measurement period and elevation angles (α) of 0°, 4°, 7°, 16°, 30°, and 90° (zenith) were selected for the scanning sequence. As there were unfortunately no measurements performed in the horizontal direction (α = 0°) during February and March, which are needed for the estimation of NO_2 and HCHO mixing ratios based on the MGA (see Sect. 3), the analysis is restricted to April, May, June, and July at this location.

After successful measurements at Zugspitze, the MAX-DOAS instrument was transferred to Pico Espejo, Venezuela and put into operation in March 2004. Measurements were then made until February 2009. Pico Espejo is located in a tropical region that is generally unperturbed by tropospheric pollution. However, Hamburger et al. (2013) observed increased aerosol amounts during the dry season by analyzing in situ measurements from the same station. They suggested that these aerosols are dominated by Venezuelan savanna fires and lifted from lower altitudes to the mountain peak. Therefore, these elevated aerosol loads can be attributed to BL air masses. At the Pico Espejo station, consecutively viewing directions of 0°, 4°, 7°, 16°, and 90° were scanned at a constant azimuth angle of 180° (south). In the year 2006, additional viewing directions were included and thus, less data for both α = 0° and α = 90° are available from that date on (see Sect. 6.2). The meteorological conditions at Pico Espejo with permanent cloud cover during the wet

season (from April to November) limit the data analysis to the dry season months December, January, February, and March.

3 Modified geometrical approach

In a recent study by Gomez et al. (2014), a modified geometrical approach (MGA) to estimate long-path averaged mixing ratios of trace gases (e.g. NO_2) from mountain MAX-DOAS measurements was proposed.

Briefly, MGA assumes a single scattering geometry and a scattering point altitude close to that of the instrument. In order to validate the former assumption, Gomez et al. (2014) performed radiative transfer model (RTM) simulations and found that the calculated hOPL for single and multiple scattering agrees within 5% for SZA < 70°. As the slant paths of the zenith (α = 90°) and horizontal (α = 0°) measurements in single scattering approximation are identical up to the scattering point, they cancel in the differential slant column density (DSCD) when using a zenith sky background spectrum close in time. The column of the trace gas in the horizontal part of the optical path can thus be determined. The MGA is a useful concept to derive free-tropospheric trace gas mixing ratios at high altitudes, where horizontal MAX-DOAS measurements are possible and aerosol loads are usually low.

The hOPL is obtained in a first step by subtracting the zenith O_4 DSCD from the horizon O_4 DSCD, divided by the number density of O_4 (n_{O4}) at the level of the station:

$$hOPL = \frac{DSCD\ (O_4,0°) - DSCD\ (O_4,90°)}{n_{O_4}}, \quad (1)$$

where n_{O4} is easily calculated by:

$$n_{O_4} = (n_{O_2})^2 = (n_{air} * 0.20942)^2 \quad (2)$$

In our study, the zenith measurements are interpolated between the solar zenith angles (SZAs) of the horizontal measurements. Thus, no further correction with respect to the differences in DSCDs due to a difference in SZA between the sequentially scans is required. The number density of air (n_{air}) at the altitude of Zugspitze and Pico Espejo is extracted from the respective

mid-latitude summer and tropical reference atmospheric model profiles of the Air Force Geophysics Laboratory (AFGL) standard atmosphere (Anderson et al., 1986).

In the second step, the mean mixing ratio of the trace gas (X_{NO2} and X_{HCHO}) is estimated for the level of the station by dividing the NO_2 and HCHO DSCD differences by the hOPL and n_{air}:

$$X_{NO_2,HCHO} = \left(\frac{DSCD\ (NO_2,HCHO,0°) - DSCD\ (NO_2,HCHO,90°)}{hOPL}\right)/n_{air} \quad (3)$$

Recently, Spinei et al. (2015) have shown that too large O_4 slant column densities are obtained when using laboratory-measured O_4 cross-sections (e.g. Hermans et al. (1999)) in low effective-temperature conditions. They report a temperature dependence in the O_4 absorption cross-section from 231 to 275 K at about 9±2.5% per 44 K rate in the 335-390 nm spectral window and suggest a small correction factor of 0.94±0.02 at 231 K when using O_4 cross-sections measured at room temperature. Following the recommendations made by Spinei et al. (2015), an overestimation of up to 6% in hOPL and thus, an underestimation in NO_2 and HCHO mixing ratios of up to 6% can be expected in our study due to the use of a room temperature O_4 cross-section.

Gomez et al. (2014) provide a detailed discussion about possible errors that may occur in the MGA. They report an error in the range of 20% for SZAs < 70°, which steeply increases to about 50% towards SZA = 80°. We follow the recommendations made by Gomez et al. (2014) and estimate hOPL as well as X_{NO2} and X_{HCHO} only for SZAs < 70°.

4 Simulation of synthetic spectra

In order to determine the effect of altitude settings and surface albedo on the O_4 DSCDs and moreover to compare the measured with simulated O_4 DSCDs at the two high altitude stations, synthetic spectra (intensities) are computed for single clear sky days using the radiative transfer model SCIATRAN, which is applied in the 1-D case (Rozanov et al., 2005).

Briefly, the software package SCIATRAN was developed for modeling radiative transfer processes in the atmosphere and ocean. The simulations can be performed for observations made by ground-based, satellite-based, ship-based, and balloon-borne instruments in the spectral range

from UV to thermal infrared. The latest release of SCIATRAN includes multiple scattering processes, polarization, thermal emission and ocean–atmosphere coupling (Rozanov et al., 2014).

The major advantage of 1-D RTMs is their low computation time and their ability to reproduce radiative transfer for clear sky conditions and over flat terrains quite well. For mountainous terrains, however, factors such as altitude and surface albedo are more difficult to treat. The computation of intensities/radiances for ground-based MAX-DOAS instruments using SCIATRAN requires, amongst others, the information on the height above sea level. For a typical measurement station in an urban area, for example, the altitude of the instrument's horizontal path (h_{path}) does not differ much from the ground level (h_{ground}) of the surrounding area (Fig. 1, left). Therefore, h_{path} would be configured by the input for h_{ground} accordingly and the position of the instrument in SCIATRAN would be set to "bottom of the atmosphere". However, for high altitude stations such as Zugspitze and Pico Espejo these settings are no longer valid as they are both located on mountain peaks and information about the atmosphere below would be lost (Fig. 1, right). Therefore, the altitude settings in SCIATRAN are adjusted by assuming that the MAX-DOAS instrument is "flying" at the respective altitude of the two measurement stations and setting the ground level to 1500 m and 150 m for Zugspitze and Pico Espejo, respectively. The latter values are chosen and optimized in approximate accordance to a representative altitude of the respective terrain in the immediate vicinity, or more specifically below the expected respective light path. The lower value selected for Pico Espejo is a result of the wide Orinoco plains in central Venezuela. For the simulations performed in this study, a surface albedo of 0.05 is used for both locations, which seems reasonable for the analyzed spring and summer season at Zugspitze and the dry season at Pico Espejo.

In addition to the altitude configurations, an extraterrestrial solar flux (Kurucz et al., 1984), a wavelength range between 330 and 410 nm, and a wavelength step of 0.4 nm are selected for the simulations. The forward model trace gases NO_2, O_3, O_4, BrO, HCHO, and SO_2, but no aerosols and clouds are implemented in the model runs. Atmospheric profiles are taken from the U.S. Standard Atmosphere 1976. The input for SZAs and solar azimuth angles (SAZs) for the selected days is taken from the MAX-DOAS measurements of the respective days. A summary of the input parameters used in SCIATRAN is given in Table 1.

5 DOAS retrieval of O_4, NO_2, and HCHO differential slant column densities

The differential optical absorption spectroscopy (DOAS) method is performed on the measured and synthetic spectra to obtain O_4, NO_2, and HCHO DSCDs, which are the parameters used for the MGA-based estimation of hOPLs as well as X_{NO2} and X_{HCHO} at the two high altitude sites.

Briefly, DOAS is based on absorption spectroscopy following Beer-Lambert's law of absorption and developed for the determination of atmospheric trace gas concentrations from remote sensing measurements of light in the UV, visible, and NIR spectral range (Platt and Stutz, 2008, and references therein). After removing the smoothly varying contributions of Mie and Rayleigh scattering from the signal, DOAS becomes sensitive to variations in absorption with wavelength. Due to the fact that individual trace gases have characteristic spectral signatures, they can be separated from the signal and quantified in terms of trace gas concentration, integrated along the atmospheric light path.

The trace gases of interest in our study, O_4, NO_2, and HCHO have spectral fingerprints in the UV and visible spectral range. As mentioned above, the spectrometer of the MAX-DOAS system at Zugspitze and Pico Espejo collected scattered sunlight between 321 and 410 nm. Therefore, the DOAS fits performed in our study are restricted to the UV.

The DOAS method is performed on the measured and synthetic spectra in the spectral range from 346-372 nm, where O_4 and NO_2 spectral fingerprints are obvious and interference with other trace gases is rather low (Platt and Stutz, 2008, and references therein). For the retrieval of HCHO, the spectral window of the DOAS analysis is shifted to 338-357 nm. Absorption cross-sections of O_3 at 223 K, NO_2 at 220 K, O_4, BrO at 223 K, and HCHO at 297 K, as well as a Ring spectrum and a polynomial of order 4 are included in the non-linear least-squares fitting procedure. For the removal of Fraunhofer lines in the solar spectrum, the measured and synthetic spectra are divided by a reference spectrum (here, a noontime spectrum at $\alpha = 90°$ with the smallest SZA is used). The resulting output of the DOAS fit is the difference in slant column amounts of O_4, NO_2, and HCHO between the measured/synthetic and reference spectrum, and

thus referred to as DSCD. A summary of fit parameters and cross-sections used for the DOAS analysis is summarized in Table 2.

An example of the spectral DOAS analysis in the 346-372 nm fitting window is shown in Fig. 2 (left) for a single spectrum, which was measured under elevated NO_2 pollution on 16th April 2003 (SZA = 37.86°, α = 0°) at Zugspitze. For the retrieval of O_4 and NO_2 DSCDs on that day, a spectrum in zenith direction (α = 90°) taken during noon (SZA = 37.36°) is used as a reference. Fit results of the DOAS analysis for the same measurement, but in the 338-357 nm fitting window yield similar values for the residuals and RMS and indicate that HCHO amounts were also higher than usual on that day (Fig.2, right).

6 Results

6.1 Measured and synthetic O_4 differential slant column densities

In this section, two sensitivity tests are carried out with the RTM SCIATRAN to determine the effect of varying altitude settings and surface albedo on the O_4 DSCDs at α = 0° and α = 90° and thus, on the estimation of hOPL. The settings used for the simulation of synthetic spectra are summarized in Table 1.

Two different altitude settings as represented schematically in Fig. 1 are used as input for SCIATRAN to simulate O_4 DSCDs at the Pico Espejo site. The resultant O_4 DSCDs as retrieved in the 346-372 nm fitting window are shown in Fig. 3 for α = 0° (red) and α = 90° (black). While the solid line represents the scenario that assumes $h_{path} = h_{ground}$, the dashed line denotes the modified settings ($h_{path} >> h_{ground}$). Clearly, the O_4 DSCDs are underestimated when the settings for common rural and/or urban measurement environments ($h_{path} = h_{ground}$) are assumed for the operation of SCIATRAN. This is the result of light path enhancements due to multiple scattering. For the horizontal viewing direction (α = 0°), the absolute difference of the two scenarios is in the order of 400 x 10^{40} $molec^2$ cm^{-5} for SZAs between 20° and 70°. The absolute differences are comparatively low for the vertical viewing direction (α = 90°), but increase towards SZA = 70° to about 100 x 10^{40} $molec^2$ cm^{-5}. Therefore, hOPL is underestimated by about 15% when the atmosphere below is cut off in the RTM.

As the Zugspitze site is located in the northern Alps at an altitude of almost 3000 m a.s.l., snow cover at the mountain peak and at lower altitudes in the immediate vicinity is common during winter and as a consequence, the surface albedo can change significantly throughout the season. Therefore, another sensitivity test with SCIATRAN is performed to evaluate the effect of a changing surface albedo on the O_4 DSCDs and the corresponding hOPL for this measurement site. The results are shown in Fig. 4 for O_4 DSCDs as retrieved in the 346-372 nm fitting window and simulated for $\alpha = 0°$ (red) and $\alpha = 90°$ (black), where the dashed and solid lines represent a surface albedo of 0.05 and 0.7, respectively, as selected for the SCIATRAN simulations. For the O_4 DSCD in the horizontal viewing direction ($\alpha = 0°$), the absolute differences are up to 400 x 10^{40} molec^2 cm^{-5} for SZAs towards 70°. Smaller absolute differences of up to 150 x 10^{40} molec^2 cm^{-5} are expected for the vertical viewing direction ($\alpha = 90°$). Consequently, a decrease in surface albedo from 0.7 to 0.05 can increase the hOPL as estimated with MGA by about 5%. The lower value of hOPL for a surface albedo of 0.7 is the result of scattering at the ground, which creates much shorter light paths. These light paths penetrate into lower levels of the atmosphere and thus, a signal of the BL could contribute to such a measurement. Consequently, measurements over brighter surfaces are less representative with respect to the analysis of trace gas amounts in the free troposphere applying the mountain DOAS approach. This has implications for the interpretation of hOPLs as estimated in mountainous terrains with changing surface albedo throughout the season.

For the comparison of O_4 DSCDs, the synthetic spectra are simulated with the modified altitude settings, which assume that the MAX-DOAS instrument is "flying" at the respective altitude of the two measurement sites and additionally include an altitude for the ground level to account for the atmosphere below the horizontal path (see Sect. 4).

The diurnal evolution of O_4 DSCDs as retrieved in the 346-372 nm fitting window are shown for single clear sky days at Zugspitze (left) and Pico Espejo (right) in Fig. 5. In general, the pattern of the measured O_4 DSCDs (red and black lines denote $\alpha = 0°$ and $\alpha = 90°$, respectively) can be reproduced by SCIATRAN (orange and gray lines denote $\alpha = 0°$ and $\alpha = 90°$, respectively) to a large extent (within 20% for SZA < 70°) for the zenith geometry at both locations. While the results show good agreement between measured and simulated horizontal O_4 DSCDs at Pico Espejo, the differences are larger at Zugspitze. The better agreement at the former station could

be explained by the higher altitude and cleaner atmosphere that is almost solely affected by Rayleigh scattering. In contrast, scattering by aerosol could play an increasing role at the altitude of the latter station. Similar results are obtained for the 338-357 nm fitting window (not shown).

6.2 Horizontal optical path length

The estimation of hOPL is based on the O_4 DSCDs in the horizontal ($\alpha = 0°$) and vertical ($\alpha = 90°$) viewing directions as obtained from the MAX-DOAS observations at Zugspitze (April till July 2003) and Pico Espejo (March 2004 till February 2009). As mentioned in Sect. 2, only the dry season months (December, January, February, and March) are considered for the analysis of hOPL and mixing ratios of NO_2 at the Pico Espejo site to avoid the cloud problem.

In Fig. 6, the estimated hOPL as derived in the 346-372 nm fitting window is shown for 16th April 2003 at the Zugspitze site and for 25th February 2005 at the Pico Espejo site. While Zugspitze was influenced by elevated NO_2 pollution in the afternoon of that day, no significant enhancements in NO_2 DSCDs are observed for Pico Espejo throughout the selected day (not shown). Clearly, the U-shaped curve of the hOPL as obtained from the measured O_4 DSCDs (dotted line) is reproduced by the simulations (solid line) and the agreement of both curves is within 10% for the Pico Espejo case. In general, one would expect smaller hOPLs from the measurements than from the simulations as performed with SCIATRAN without the inclusion of aerosols (see Table 1). One possible explanation for the higher measured values at Pico Espejo could be an aerosol layer below the measurement site. The differences are much larger for the case at Zugspitze. While the differences are about 25% in the morning, they rise to 70% in the afternoon, where NO_2 pollution increased as well (see Sect. 6.1). Again, the better agreement at Pico Espejo might be related to the higher altitude and cleaner atmosphere with negligible Mie scattering.

Gomez et al. (2014) have simulated the hOPL for a single wavelength in the visible spectral range (440 nm) and also found a U-shaped curve with higher values of hOPL towards larger SZAs. However, the distances estimated in their study are larger by a factor of about two, although the Izaña station is located at a lower altitude (2373 m a.s.l.) than the Zugspitze and

Pico Espejo sites. This means that trace gas concentrations are averaged over a shorter distance in the UV than in the visible, even at higher altitudes. Consequently, MAX-DOAS measurements in the UV are representative of free-tropospheric trace gas concentrations to a lesser extent than in the visible as the influence of BL air masses that are lifted to the station is larger for the shorter horizontal path. Nevertheless, the hOPL in the UV during clear sky conditions is still sufficiently long that NO_2 close to the station is considered to have a negligible influence.

The hOPLs as derived in the 346-372 nm are illustrated in Fig. 7 for the entire period at Zugspitze (April till July 2003) and for one dry season at Pico Espejo (January 2005 till March 2005) in the upper and lower panels, respectively. Clearly, higher hOPL values are obtained from the measurements at Pico Espejo (> 40 km) than for those at Zugspitze (> 20 km), which is simply explained by the higher elevation of the former station. While the highest values are observed during clear sky conditions, low hOPLs are generally connected to clouds. Negative values arise when the retrieved O_4 DSCD at $\alpha = 0°$ is negative or lower than O_4 DSCD at $\alpha = 90°$, which can happen due to thick stratus clouds with cloud top heights that overtop the altitude of the station and thus, particularly affect the horizontal MAX-DOAS measurements.

Since the estimation of NO_2 and HCHO mixing ratios only makes sense when the sky in the horizontal and vertical viewing directions is neither influenced by clouds nor by high aerosol amounts, the data are filtered for clear sky cases. For further analyses, only those hOPL values are considered where the root mean square (RMS) error of the DOAS fit for $\alpha = 0°$ is smaller than 5×10^{-4}, O_4 and NO_2/HCHO DSCDs in the vertical viewing direction ($\alpha = 90°$) are positive, and NO_2/HCHO DSCDs at $\alpha = 90°$ are smaller than NO_2/HCHO DSCDs at $\alpha = 0°$. As no instruments to obtain information on atmospheric visibility were available at the stations, we have tested different lower limits of hOPL as a filter criterion and found that 17.5 km and 30 km in the 346-372 nm fitting window and 12.5 km and 22.5 km in the 338-357 nm fitting window are good compromises for Zugspitze and Pico Espejo, respectively (see Fig. 7). All data points falling below these thresholds are attributed to high aerosol amounts and/or clouds and thus, are removed from the analysis of mixing ratios. As mentioned in Sect. 3, only data for SZA < 70° are included in the analysis. Due the fact that cloudiness is common at Zugspitze during spring and summer (April till July 2003), the absolute number of data points is vastly reduced from 11112 to 366 (320) after applying these filter criteria in the 346-372 nm (338-357 nm) fitting window.

Nevertheless, the remaining data are of good quality and provide important insights into the free troposphere at this station with respect to hOPL, X_{NO2}, and X_{HCHO}. The loss of data is considerably less for the Pico Espejo site, where the absolute number of data points decreases from 8364 to 1700 (1682), 10258 to 944 (354), 2432 to 371 (142), 3019 to 563 (273), and 2081 to 315 (140) in the 346-372 nm (338-357 nm) fitting window after applying the filter criteria for the dry seasons (December till March) of the years 2004/05, 2005/06, 2006/07, 2007/08, and 2008/2009, respectively.

The monthly means (April, May, June and July 2003) and multi-year averaged (2004-2009) monthly means (December till March) of hOPL as derived in the 346-372 nm fitting window for clear sky conditions as defined in the paragraph above are shown in Fig. 8 as a function of aerosol optical depth (AOD) for Zugspitze (left) and Pico Espejo (right), respectively. AOD is defined as the integrated extinction coefficient over a vertical column and thus, does not say anything about the vertical profile of the aerosol load. As for NO_2, most of the aerosol load is located in the BL and generally close to its sources. For example, Gonzi et al. (2015) have estimated biomass burning injection heights using active fire area and fire radiative power from MODIS data in combination with a parameterized plume rise model. They found that 80% of the injections remain within the local boundary layer. Consequently, trace gases and aerosols are only lifted into the free troposphere when the active fire area and convective heat flux exceed a certain threshold. For the Pico Espejo site, it is expected that the possibility of injections reaching the free troposphere increases towards the end of the dry season with increasing fire activity. Due to a lack of ground-based measurements of AOD at the two stations that are representative for the altitude of the station, monthly gridded means of AOD from the MODIS instrument on board Terra and Aqua satellites have been downloaded from ftp://ladsweb.nascom.nasa.gov/allData/51/ (Remer et al., 2008) and averaged over both products and selected regions (see Table 3). The MODIS instruments have 36 channels covering the spectral range from 410 to 14400 nm and representing three different spatial resolutions of 250 m, 500 m, and 1 km. The AOD product used in our study is retrieved at 550 nm and has a spatial resolution of 250 m. Again, the MODIS product provides an extinction coefficient integrated over a vertical column with probably most of the aerosol load being located below the measurement stations. Nevertheless, the effect of aerosols on hOPL can still be quantified for the Pico Espejo site as about 20% of the aerosol load

is expected to be found in the free troposphere, following the recommendations made by Gonzi et al. (2015). While the estimated hOPLs increase throughout the season at Zugspitze, the results show a decrease of hOPLs towards the end of the dry season at Pico Espejo (Fig. 8). Clearly, AOD seems to be the main driver affecting hOPL in both cases. The decrease in AOD at Zugspitze might be due to an overall decrease in residential wood burning towards summer time in that region (Szidat et al., 2007). On the other hand, the increase in AOD at Pico Espejo is connected to increased biomass burning towards the end of the dry season in that region (Hamburger et al., 2013). Interestingly, there is no relationship between hOPL and AOD observed for the 338-357 nm fitting window (see Table 3). One reason could be the larger uncertainties in O_4 DSCDs, which are used to obtain hOPL.

6.3 Long-path averaged NO_2 mixing ratios

The monthly averaged X_{NO2} as a function of AOD and the multi-year averaged monthly means of X_{NO2} as a function of fire radiative power (FRP) are shown in Fig. 9 for Zugspitze (left) and Pico Espejo (right), respectively. FRP is defined as the radiant component of energy release from a fire (Kaufmann et al., 1998).

Monthly averaged values of X_{NO2} at Zugspitze are 93.5±49.8 ppt and 102±60.5 ppt in the spring months April and May, respectively, whereas lower values of 59.6±55.6 and 61.8±28.9 ppt are derived for the summer months June and July. As pollution at the Zugspitze site is mainly anthropogenically induced, the general co-occurrence of higher AOD and higher X_{NO2} is not surprising. Clearly, higher values of X_{NO2} are observed during the spring months April and May, which could be explained by both higher combustion due to residential burning and longer life time of NO_2. While the values of the months April, May, and July are linearly related to a large extend, either AOD is higher or X_{NO2} is lower than expected from the linear relation in June. This slight deviation could be related to the fact that air masses with less NO_2 and/or more aerosols crossed the light path of the instrument in June. However, no significant differences in the origin of air masses between the different months could be found by exploring back-ward trajectories for the days of measurements that remain after applying the filter criteria to the data (not shown). The y-intercept of the linear least-squares fit (excluding June) in the order of 20 ppt (not shown)

provides some information on the background levels of X_{NO2} in this region and at this altitude. In comparison, Gomez et al. (2014) and Gil-Ojeda et al. (2015) have reported NO_2 mixing ratios between 20 ppt and 45 ppt for the clean subtropical FT at a similar altitude, which is in good agreement with the background value obtained for Zugspitze, which is located more than 2000 km north of the Izaña station.

The multi-year averaged values of X_{NO2} for the higher elevated station Pico Espejo are somewhat smaller when compared to X_{NO2} values at Zugspitze (Table 3). As observed for Zugspitze, there is a positive linear relationship with AOD (not shown), suggesting a background value of 5.5 ppt. The multi-year averaged values of X_{NO2} as a function of multi-year averaged FRP is illustrated in Fig. 9. Clearly, X_{NO2} increases with increasing fire activity towards the end of the dry season. The calculation of a linear least-squares fit reveals a y-intercept of 4 ppt, which is in agreement with the y-intercept as derived for X_{NO2} vs. AOD.

Although the long-path averaged NO_2 mixing ratios at Pico Espejo are estimated at an altitude of almost 5000 m a.s.l., and thus, clearly above the boundary layer, it seems that the FT is regularly affected by biomass burning emissions in this region.

X_{NO2} as retrieved in the 346-372 nm fitting window (blue) is compared with X_{NO2} as derived in the 338-357 nm fitting window (red) for a polluted day at Zugspitze (see Fig. 10). In general, the shape of both curves is similar to a large extend with lowest (highest) values observed in the morning (late afternoon). Although the spectral signatures of NO_2 and O_4 are less pronounced and interference with other gases is stronger in the 338-357 nm fitting window, mixing ratios of NO_2 are still in good agreement with X_{NO2} obtained in the 346-372 nm fitting window.

6.4 Long-path averaged HCHO mixing ratios

The same analysis that was applied to derive NO_2 mixing ratios in the free troposphere was also applied to HCHO. Due to its characteristic spectral signatures at lower wavelengths, the retrieval of HCHO is shifted to the spectral range from 338-357 nm (see Sect. 5 and Table 2).

In Figure 11, the diurnal evolution of HCHO DSCDs as retrieved in the 338-357 nm fitting window for $\alpha = 0°$ (red) and $\alpha = 90°$ (black) is shown for the same day at Zugspitze. As observed for NO_2, HCHO levels increase in the afternoon. Backward trajectories as calculated with the Hybrid Single-Particle Lagrangian Integrated Trajectory (HYSPLIT) online tool (Draxler and Rolph, 2013) using meteorological data from the NCEP/NCAR 40-year reanalysis project (Kalnay et al., 1996) indicate that air masses from a more densely populated region at lower elevation in the northeast moved along the slope of the Bavarian alps, before crossing the light path of the MAX-DOAS instrument (not shown). While the increase of HCHO DSCD is obvious for $\alpha = 0°$ (red), HCHO DSCD at 90° (black) is relatively stable throughout the day with slightly negative columns obtained in the morning hours.

The filter criteria, as defined in Sect. 6.2 are applied to obtain X_{HCHO} during clear sky conditions. An exemplary diurnal evolution of X_{HCHO} before (green) and after (black) applying the filter criteria is shown for the polluted day at Zugspitze in Fig. 12. According to the filter criteria, the remaining black dots are observed during clear sky conditions and are in the range of 400-800 ppt.

Monthly means of X_{HCHO} between April and July are in the range of 500-950 ppt at the Zugspitze site (Table 3). Air sampling of HCHO deduced from a flight track of the TROPospheric OZone Experiment (TROPOZ-2) above Northern Spain/Western France reveals HCHO mixing ratios of ~400 ppt at a similar altitude, but in the winter season (Arlander et al., 1995). According to the seasonal variability of HCHO in the mid-latitudes as obtained from satellite measurements, lowest values of HCHO are observed during winter months (De Smedt et al., 2015). Therefore, the higher values observed in our study during spring and summer months are reasonable. Considerable lower HCHO mixing ratios at Zugspitze are found in April when compared with values in May, June, and July. This is in good agreement with HCHO concentrations as obtained from MAX-DOAS measurements at the high-alpine station Jungfraujoch (Franco et al., 2015). In both cases, the April values are about 35% lower than the average of May, June, and July values.

Multi-year averaged monthly means of X_{HCHO} as obtained during the dry season at Pico Espejo are in the range of 255-385 ppt and thus, well below the values deduced at Zugspitze. The comparison with HCHO deduced from air sampling in this region during TROPOZ-2 is quite

revealing, with our values being slightly higher at this altitude. Singh et al. (2001) reported values of HCHO mixing ratios in the range of 100-200 ppt for this altitude. However, they have used data from a larger region (0-30°S, 165°E-100°W) and focused on the tropospheric composition over the tropical Pacific Ocean.

7 Summary and conclusions

In this study, Multi-AXis Differential Optical Absorption Spectroscopy (MAX-DOAS) data sets from two high altitude stations in the mid-latitudes and tropics are analyzed for horizontal optical path lengths (hOPLs) and free-tropospheric NO_2 (X_{NO2}) and HCHO (X_{HCHO}) mixing ratios. The method is based on the modified geometrical approach (MGA), which assumes a single-scattering geometry and a scattering point altitude close to the instrument altitude.

For the estimation of hOPL, X_{NO2}, and X_{HCHO}, DSCDs of O_4, NO_2, and HCHO in the horizontal (0°) and vertical (90°) viewing directions are obtained with a conventional differential optical absorption spectroscopy (DOAS) retrieval between 346 and 372 nm for the NO_2 and between 338 and 357 nm for the HCHO retrieval. In order to compare the O_4 DSCDs with synthetic data and moreover to evaluate the effect of a varying surface albedo on the O_4 DSCDs, the radiative transfer model SCIATRAN is used. As for the retrieval of O_4 DSCDs from MAX-DOAS measurements, the synthetic spectra are also analyzed with the DOAS method.

In general, the measured and synthetic vertical O_4 DSCDs are in good agreement (differences < 20%) during clear sky conditions and for solar zenith angles (SZA) smaller than 70°. While the differences between measured and synthetic horizontal O_4 DSCDs are small at the higher and "cleaner" Pico Espejo site (< 10%), they are between 25% and 70% at Zugspitze. The results of the sensitivity analyses show that a decrease in surface albedo from 0.7 to 0.05 can increase hOPL by about 5%, which can have possible implications for such measurements in mountainous terrains with a seasonal varying snow cover.

Monthly means and multi-year averaged monthly means of hOPL as obtained from the long-term measurements are 19 km (14 km) and 34 km (26.5 km) for the 346-372 nm (338-357 nm) fitting window at Zugspitze and Pico Espejo, respectively. At both high altitude sites, hOPL as derived

in the 346-372 nm fitting window decreases as a function of increasing aerosol amounts. In contrast, no relationship is found for the 338-357 nm fitting window, which could be explained by the larger uncertainties in O_4 DSCDs.

Long-path averaged mixing ratios of NO_2 are obtained using the estimated hOPL. The monthly means and multi-year averaged monthly means of X_{NO2} are in the range of 60-100 ppt and 8.5-15.5 ppt at Zugspitze and Pico Espejo, respectively. A statistically significant linear relationship between aerosol optical depth (AOD) and X_{NO2} is obtained for the measurements from both measurement sites, suggesting that both NO_2 and aerosols are closely connected to air pollution in these regions and at the respective altitude level. The results of a linear least-squares fit performed on the averaged data show that upper limits for the background free troposphere NO_2 mixing ratios are about 20 ppt and 4.5 ppt for Zugspitze and Pico Espejo, respectively, where the former value is in good agreement with background NO_2 mixing ratios reported by Gomez et al. (2014) and Gil-Ojeda et al. (2015) for a similar altitude at the Izaña station (28.3°N, 16.48°W, 2373 m a.s.l.). The latter site on Tenerife is relatively remote, whereas Zugspitze is farther north but both are probably probing on average similar free tropospheric air masses transported from Tenerife towards Europe. However, the higher values at mid-latitudes in the northern hemisphere as opposed to those close to the ITCZ are probably indicating an anthropogenic influence at mid-latitudes in the free troposphere.

The same procedure as for X_{NO2} is applied to obtain X_{HCHO}, but for an optimized fitting window covering the strong spectral signatures of HCHO. The monthly means of X_{HCHO} at the Zugspitze site are 500-950 ppt, which is reasonable when comparing these values with values obtained from air sampling in winter at similar altitudes and latitudes as well as considering a seasonal variability in this region. At mid-latitudes, the values of HCHO and NO_2 are relatively high for clean conditions. This implies that there is sufficient NO_x for oxidizing hydrocarbons through photooxidative catalytic cycles. As a consequence, production of some tropospheric ozone (O_3) is occurring at mid-latitudes in the free troposphere. The values of X_{HCHO} are in the range of 255-385 ppt at Pico Espejo and increase towards the end of the dry season. Moreover, multi-year averaged monthly means of X_{HCHO} are linearly correlated with the multi-year averaged monthly means of X_{NO2}, further supporting the notion that emissions from South American biomass burning clearly reach the free troposphere in this region. This probably also implies some

photooxidation of hydrocarbons and production of O_3 is occurring some of the time in the air masses observed in the free troposphere above Pico Espejo.

Acknowledgements

This study was funded by the University of Bremen. The set-up and operation of the MAX-DOAS instrument on Zugspitze and Pico Espejo was funded by DLR Bonn in the framework of SCIAMACHY validation. We would like to thank Thomas Medeke, Sixten Fietkau and Astrid Loewe for their work on the DOAS instruments and data and NASA for the provision of MODIS data.

References

Anderson, G., Clough, S., Kneizys, F., Chetwynd, J., and Shettle, E.: AFGL atmospheric constituent profiles (0–120 km), Tech. Rep. AFGL-TR-86-0110, Air Force Geophys. Lab., Hanscom Air Force Base, Bedford, Mass., 1986.

Anderson, L. G., Lanning, J. A., Barrell, R., Miyagishima, J., Jones, R. H., and Wolfe, P: Sources and sinks of formaldehyde and acetaldehyde: an analysis of Denver's ambient concentration data, Atmos. Environ., 30, 12, 2113–2123, 1996.

Andreae, M. O. and Merlet, P.: Emission of trace gases and aerosols from biomass burning, Global Biogeochem. Cy., 15, 955–966, 2001.

Arlander, D. W., Brüning, D., Schmidt, U., and Ehhalt, D. H.: The tropospheric distribution of formaldehyde during TROPOZ II, J. Atmos. Chem., 22, 251–268, 1995.

Choi, S., Joiner, J., Choi, Y., Duncan, B. N., Vasilkov, A., Krotkov, N., and Bucsela, E.: First estimates of global free-tropospheric NO2 abundances derived using a cloud-slicing technique applied to satellite observations from the Aura Ozone Monitoring Instrument (OMI), Atmos. Chem. Phys., 14, 10565–10588, doi:10.5194/acp-14-10565-2014, 2014.

De Smedt, I., Stavrakou, T., Hendrick, F., Danckaert, T., Vlemmix, T., Pinardi, G., Theys, N., Lerot, C., Gielen, C., Vigouroux, C., Hermans, C., Fayt, C., Veefkind, P., Müller, J.-F., and Van Roozendael, M.: Diurnal, seasonal and long-term variations of global formaldehyde columns inferred from combined OMI and GOME-2 observations, Atmos. Chem. Phys. Discuss., 15, 12241-12300, doi:10.5194/acpd-15-12241-2015, 2015.

Draxler, R. R., and Rolph, G. D.: HYSPLIT (HYbrid Single-Particle Lagrangian Integrated Trajectory) Model access via NOAA ARL READY Website, available at: http://www.arl.noaa.gov/HYSPLIT.php (last access: May 2014). NOAA Air Resources Laboratory, College Park, MD, 2013.

Fleischmann, O. C., Hartmann, M., Burrows, J. P., and Orphal, J.: New ultraviolet absorption cross-sections of BrO at atmospheric temperatures measured by time-windowing Fourier transform spectroscopy, J. Photochem. Photobiol. A: Chemistry, 168, 117–132, doi:10.1016/j.jphotochem.2004.03.026, 2004.

Franco, B., Hendrick, F., Van Roozendael, M., Müller, J., Stavrakou, T., Marais, E. A., Bovy, B., and Bader, W.: Retrievals of formaldehyde from ground-based FTIR and MAX-DOAS observations at the Jungfraujoch station and comparisons with GEOS-Chem and IMAGES model simulations, Atmos. Meas. Tech., 8, 1733–1756, doi:10.5194/amt-8-1733-2015, 2015.

Fried, A., Crawford, J., Olson, J., Walega, J., Potter, W., Wert, B., Jordan, C., Anderson, B., Shetter, R., Lefer, B., Blake, D., Blake, N., Meinardi, S., Heikes, B., O'Sullivan, D., Snow, J., Fuelberg, H., Kiley, C. M., Sandholm, S., Tan, D., Sachse, G., Singh, H., Faloona, I., Harward, C. N. and Carmichael, G.R.: Airborne tunable diode laser measurements of formaldehyde during TRACEP: Distributions and box model comparisons. J. Geophys. Res.-Atmos., 108 (D20), 8798, doi:10.1029/2003JD003451, 2003.

Gil-Ojeda, M., Navarro-Comas, M., Gómez-Martín, L., Adame, J. A., Saiz-Lopez, A., Cuevas, C. A., González, Y., Puentedura, O., Cuevas, E., Lamarque, J.-F., Kinninson, D., and Tilmes, S.: NO2 seasonal evolution in the north subtropical free troposphere, Atmos. Chem. Phys., 15, 10567-10579, doi:10.5194/acp-15-10567-2015, 2015.

Gomez, L., Navarro-Comas, M., Puentedura, O., Gonzalez, Y., Cuevas, E., and Gil-Ojeda, M.: Long-path averaged mixing ratios of O3 and NO2 in the free troposphere from mountain MAX-DOAS, Atmos. Meas. Tech., 7, 3373–3386, doi: 10.5194/amt-7-3373-2014, 2014.

Gonzi, S., Palmer, P. I., Paugam, R., Wooster, M., and Deeter, M. N.: Quantifying pyroconvective injection heights using observations of fire energy: sensitivity of spaceborne observations of carbon monoxide, Atmos. Chem. Phys., 15, 4339-4355, doi:10.5194/acp-15-4339-2015, 2015.

Guenther, A., Karl, T., Harley, P., Wiedinmyer, C., Palmer, P. I., and Geron, C.: Estimates of global terrestrial isoprene emissions using MEGAN (Model of Emissions of Gases and Aerosols from Nature), Atmos. Chem. Phys., 6, 3181–3210, doi:10.5194/acp-6-3181-2006, 2006.

Hamburger, T., Matisans, M., Tunved, P., Ström, J., Calderon, S., Hoffmann, P., Hochschild, G., Gross, J., Schmeissner, T., Wiedensohler, A., and Krejci, R.: Long-term in situ observations of biomass burning aerosol at a high altitude station in Venezuela – sources, impacts and interannual variability, Atmos. Chem. Phys., 13, 9837–9853, doi: 10.5194/acp-13-9837-2013, 2013.

Hermans, C., Vandaele, A., Carleer, M., Fally, S., Colin, R., Jenouvrier, A., Coquart, B., and Mérienne, M.-F.: Absorption cross-sections of atmospheric constituents: NO2, O2, and H2O, Environ. Sci. Pollut. Res., 6, 151–158, doi:10.1007/BF02987620, 1999.

Hönninger, G., von Friedeburg, C., and Platt, U.: Multi axis differential optical absorption spectroscopy (MAX-DOAS), Atmos. Chem. Phys., 4, 231–254, doi:10.5194/acp-4-231-2004, 2004.

Kalnay, E., Kanamitsu, M., Kistler, R., Collins, W., Deaven, D., Gandin, L., Iredell, M., Saha, S., White, G., Woollen, J., Zhu, Y., Leetmaa, A., Reynolds, R., Chelliah, M., Ebisuzaki, W., Higgins, W., Janowiak, J., Mo, K. C., Ropelewski, C., and Wang, J.: The NCEP/NCAR 40-year reanalysis project, B. Am. Meteorol. Soc., 77, 437–470, 1996.Kaufman, Y. J., Justice, C. O., Flynn, L. P., Kendall, J. D., Prins, E. M., Giglio, L., Ward, D. E., Menzel, W. P., and Setzer, A. W.: Potential global fire monitoring from EOS-MODIS, J. Geophys. Res.-Atmos., 103, 32215–32238, 1998.

Kritten, L., Butz, A., Dorf, M., Deutschmann, T., Kühl, S., Prados-Roman, C., Puķīte, J., Rozanov, A., Schofield, R., and Pfeilsticker, K.: Time dependent profile retrieval of UV/vis absorbing radicals from balloon-borne limb measurements – a case study on NO2 and O3, Atmos. Meas. Tech., 3, 933-946, doi:10.5194/amt-3-933-2010, 2010.

Kurucz, R. L., Furenhild, I., Brault, J., and Testermann, L.: Solar flux atlas from 296 to 1300 nm, National Solar Observatory Atlas No. 1, June 1984, 1984.

Lee, D. S., Köhler, I., Grobler, E., Rohrer, F., Sausen, R., Gallardo- Klenner, L., Olivier, J. G. J., Dentener, F. J., and Bouwman, A. F.: Estimations of global NO(x) emissions and their uncertainties, Atmos. Environ., 31, 1735–1749, 1997.

Lowe, D. C. and Schmidt, U.: Formaldehyde (HCHO) measurements in the nonurban atmosphere, J. Geophys. Res., 88(15), 844–858, 1983.

Meller, R. and Moortgat, G. K.: Temperature dependence of the absorption cross sections of formaldehyde between 223 and 323 K in the wavelength range 225–375 nm, J. Geophys. Res., 105, 7089–7101, doi:10.1029/1999JD901074, 2000.

Oetjen, H.: Measurement of halogen oxides by scattered sunlight differential optical absorption spectroscopy, PhD thesis, University of Bremen, Germany, available at: http://www.iup.uni-bremen.de/doas/paper/diss_oetjen_2009.pdf (last access: 2.12.2015), 2009.

Peters, E.: Improved MAX-DOAS measurements and retrievals focused on the marine boundary layer, PhD thesis, University of Bremen, Germany, available at: http://www.iup.uni-bremen.de/doas/paper/diss_peters_2013.pdf (last access: 2.12.2015), 2013.

Platt, U. and Stutz, J.: Differential Optical Absorption Spectroscopy. Physics of Earth and Space Environments, Springer, Berlin, 2008.

Reidmiller, D. R., Jaffe, D. A., Fischer, E. V., and Finley, B.: Nitrogen oxides in the boundary layer and free troposphere at the Mt. Bachelor Observatory, Atmos. Chem. Phys., 10, 6043–6062, doi: 10.5194/acp-10-6043-2010, 2010.

Remer, L. A., Kleidman, R. G., Levy, R. C., Kaufman, Y. J., Tanré, D., Mattoo, S., Martins, J. V., Ichoku, C., Koren, I., Yu, H., and Holben, B. N.: Global aerosol climatology from the MODIS satellite sensors, J. Geophys. Res.-Atmos., 113, D14S07, doi:10.1029/2007JD009661, 2008.

Rozanov, A., Rozanov, V. V., Buchwitz, M., Kokhanovsky, A. A., and Burrows, J. P.: SCIATRAN 2.0 – a new radiative transfer model for geophysical applications in the 175– 2400 nm spectral region, Adv. Space Sci., 36, 1015–1019, doi:10.1016/j.asr.2005.03.012, 2005.

Rozanov, V., Rozanov, A., Kokhanovsky, A., and Burrows, J.: Radiative transfer through terrestrial atmosphere and ocean: Software package SCIATRAN, J. Quant. Spec. R. Trans., doi: 10.1016/j.jqsrt.2013.07.004, 2014.

Schuster, G., Wilson, S., and Helas, G.: Formaldehyde measurements in the free troposphere, in: Physico-Chemical Behaviour of Atmospheric Pollutants, G. Restelli & G. Angeletti (Eds.), Kluwer Academic Publishers, Dordrecht/Boston-London 1990, pp. 553-557, 1990.

Seco, R., Penuelas, J., and Filella, I.: Short-chain oxygenated VOCs: Emission and uptake by plants and atmospheric sources, sinks, and concentrations, Atmos. Environ., 41, 2477–2499, 2007.

Serdyuchenko, A., Gorshelev, V., Weber, M., Chehade, W., and Burrows, J. P.: High spectral resolution ozone absorption cross-sections – Part 2: Temperature dependence, Atmos. Meas. Tech., 7, 625-636, doi:10.5194/amt-7-625-2014, 2014.

Singh, H., Chen, Y., Staudt, A., Jacob, D., Blake, D., Heikes, B., and Snow, J.: Evidence from the Pacific troposphere for large global sources of oxygenated organic compounds, Nature, 410, 1078–1081, 2001.

Singh, H. B., Brune, W. H., Crawford, J. H., Flocke, F., and Jacob, D. J.: Chemistry and transport of pollution over the Gulf of Mexico and the Pacific: spring 2006 INTEX-B campaign overview and first results, Atmos. Chem. Phys., 9, 2301–2318, 2009.

Szidat, S., Prevot, A. S. H., Sandradewi, J., Alfarra, M. R., Synal, H.-A., Wacker, L., and Baltensperger, U.: Dominant impact of residential wood burning on particulate matter in

Alpine valleys during winter, Geophys. Res. Lett., 34, L05820, doi:10.1029/2006GL028325, 2007.

Vandaele, A. C., Hermans, C., Simon, P. C., Roozendael, M. V., Guilmot, J. M., Carleer, M., and Colin, R.: Fourier transform measurement of NO2 absorption cross-section in the visible range at room temperature, J. Atmos. Chem., 25, 289–305, 1996.

Weller, R., Schrems, O., Boddenberg, A., G¨ab, S., and Gautrois, M.: Meridional distribution of hydroperoxides and formaldehyde in the marine boundary layer of the Atlantic (48N–35S) measured during the Albatross campaign, J. Geophys. Res., 105(D11), 14401–14412, 2000.

Wittrock, F., Oetjen, H., Richter, A., Fietkau, S., Medeke, T., Rozanov, A., and Burrows, J. P.: MAX-DOAS measurements of atmospheric trace gases in Ny-Ålesund – Radiative transfer studies and their application, Atmos. Chem. Phys., 4, 955–966, doi:10.5194/acp-4-955-2004, 2004.

WMO: GAW Report No. 189: Report of the MACC/GAW Session on the Near-Real-Time Delivery of the GAW Observations of Reactive Gases, Garmisch-Partenkirchen, Germany, 6–8 October 2009, available at: http://www.wmo.int/pages/prog/arep/gaw/documents/WMO_TD_No_1527_GAW_189_web.pdf (last access: 8.10.2015), 2010.

Table 1. Parameter settings used for the computation of synthetic spectra with the radiative transfer model SCIATRAN.

	SCIATRAN input
RTM mode	Intensity/radiance
RTM type	Spherical atmosphere
Extraterrestrial solar flux	Solar atlas (Kurucz et al., 1984)
Wavelength range	330-410 nm (UV)
Wavelength step	0.04 nm
Forward model trace gases	NO_2, O_3, O_4, BrO, HCHO, and SO_2
Aerosols	No aerosols
Clouds	No clouds
"Flying" altitude	4765 m (Pico Espejo), 2650 m (Zugspitze)
"Ground" altitude	150 m (Pico Espejo), 1500 m (Zugspitze)
Surface albedo	0.05
	SCIATRAN observation geometry
Solar zenith angles	From MAX-DOAS observations
Solar azimuth	From MAX-DOAS observations
Elevation angles	0°, 4°, 7°, 16°, 30°, and 90° (zenith)

Table 2. Fit parameters and cross-sections included in the spectral fitting procedure.

Fit parameter		**Selection**
Spectral range		346-372 nm (NO_2), 338-357 nm (HCHO)
Polynomial degree		4
Wavelength calibration		Solar atlas (Kurucz et al., 1984)
Reference		Noontime spectrum with smallest SZA
Cross section	**Temperature**	**Data source**
O_3	223 K	Serdyuchenko et al. (2014)
NO_2	296 K	Vandaele et al. (1996)
O_4	296 K	Hermans et al. (1999)
BrO	223 K	Fleischmann et al. (2004)
HCHO	297 K	Meller and Moortgat (2000)
Ring	-	SCIATRAN

Table 3. Arithmetic mean and standard deviation of the parameters hOPL, X_{NO2}, and X_{HCHO} as estimated from the high altitude MAX-DOAS measurements as well as aerosol optical depth (AOD) and fire radiative power (FRP) from MODIS on board Terra and Aqua satellites. Both AOD and FRP are averages over monthly means obtained from MODIS on board Terra (10:30 LT) and Aqua (13:30 LT) satellites. The standard deviation of daily and monthly means is given for Zugspitze and Pico Espejo, respectively, and the numbers in brackets are latitude and longitude as defined for the regions selected for spatially averaging AOD and FRP.

	Zugspitze (47° to 49°N, 11° to 13°E)				**Pico Espejo (8° to 11°N, 72° to 69°W)**			
	April	**May**	**June**	**July**	**December**	**January**	**February**	**March**
hOPL [km] (338-357 nm)	15.1±1.7	14.4±1.4	13.7±1	14.6±2.1	26.2±1.2	26.8±1.5	26.3±1.9	26.7±1.4
hOPL [km] (346-372 nm)	19.1±1.3	19.3±1.3	19±1.4	19.6±1.4	34.7±0.6	34.3±0.6	34.1±0.5	32.8±1.4
AOD	0.25±0.12	0.22±0.13	0.23±0.1	0.14±0.09	0.11±0.03	0.12±0.02	0.16±0.04	0.35±0.04
XNO_2 [ppt] (346-372 nm)	93.5±49.8	102±60.5	59.6±55.6	61.8±28.9	8.4±4.2	8.6±3.5	10.5±5.4	15.4±3.9
XHCHO [ppt] (338-357 nm)	497±123	640±277	947±395	634±441	262±23.5	254±36.8	280±51.8	385±38.6
FRP [mW m^{-2}]	-	-	-	-	6.8±1.74	12.3±2.54	17.9±3.97	21.9±3.65

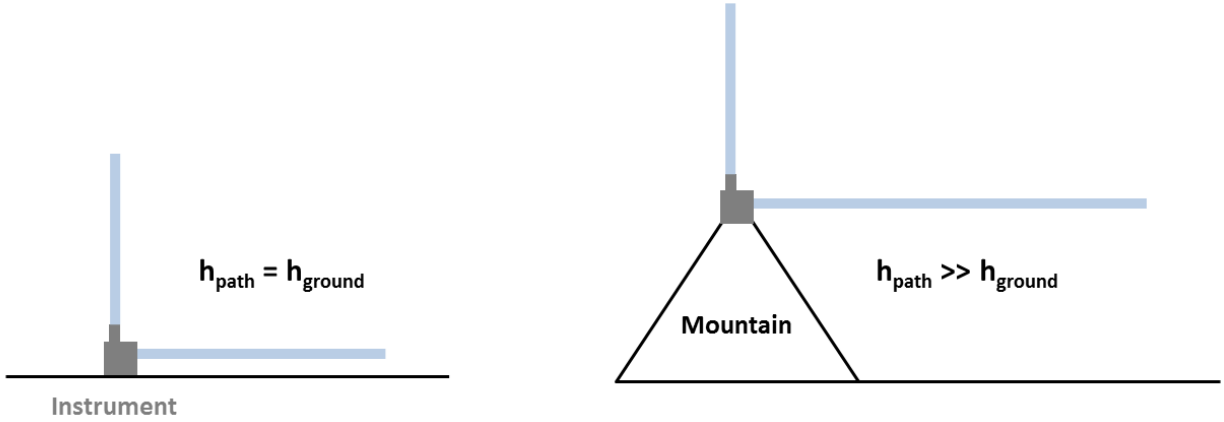

Figure 1. Schematic illustration of the MAX-DOAS observation geometry in a typical urban and/or rural setting (left) and in a mountainous terrain (right). While the altitude of the instrument's horizontal path (h_{path}) corresponds to the ground level (h_{ground}) of the surrounding area in the left sketch, h_{path} is larger than h_{ground} in the right graph.

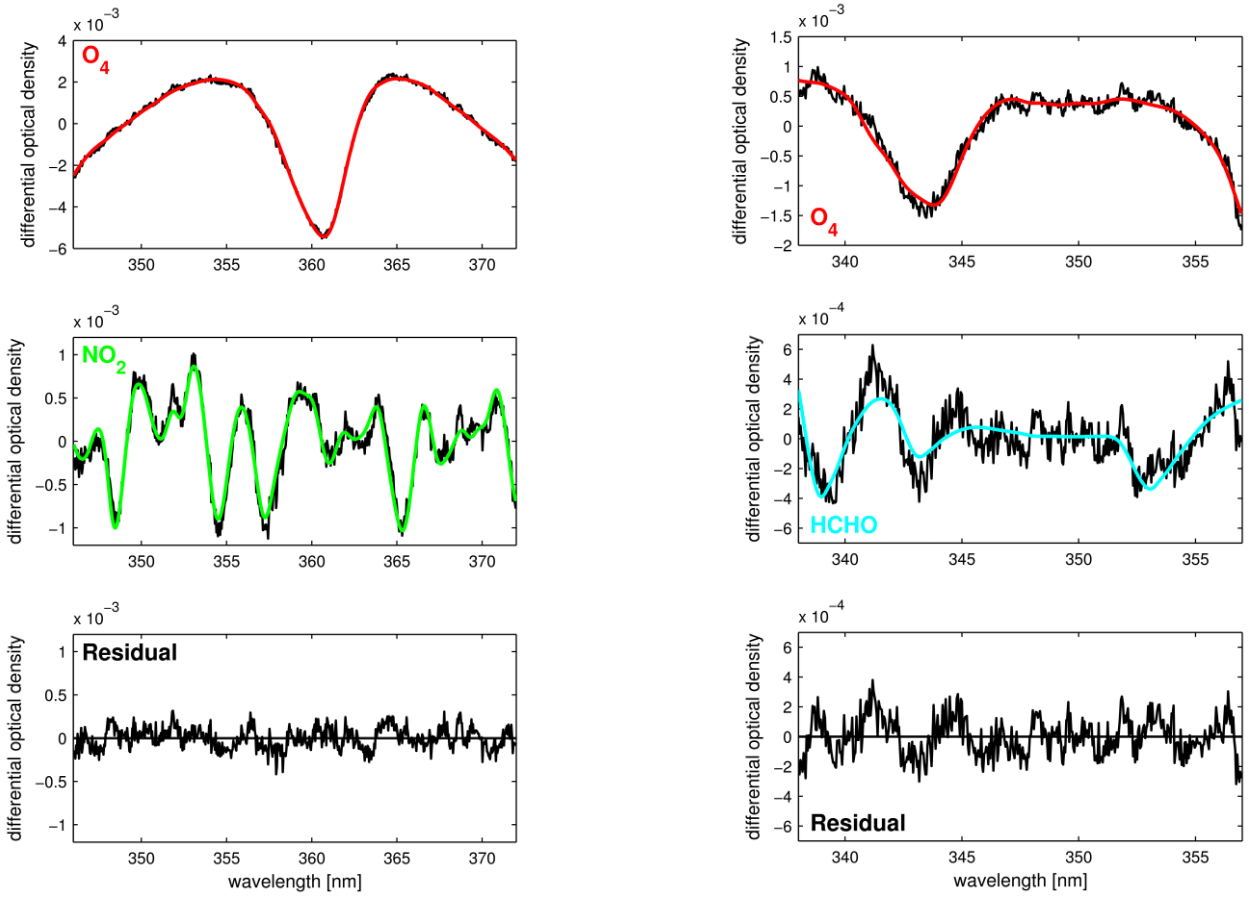

Figure 2. Exemplary fit results of the DOAS analysis in the 346-372 nm (left) and 338-357 nm (right) fitting window for a horizontal noontime MAX-DOAS spectrum (α = 0°, SZA = 37.86°) as measured on 16th April 2003 at Zugspitze under elevated NO_2 (DSCD = 1.228 x 10^{16} molec cm^{-2}) and HCHO (DSCD = 1.737 x 10^{16} molec cm^{-2}) pollution. The red (upper panel), green and cyan (middle panel) lines show the O_4, NO_2 and HCHO cross sections, respectively, as scaled to the O_4, NO_2 and HCHO absorptions detected in the measured spectrum (black lines). The residuals with calculated root mean square (RMS) errors of 1.2 x 10^{-4} (346-372 nm) and 1.3 x 10^{-4} (338-357 nm) are also shown (lower panel).

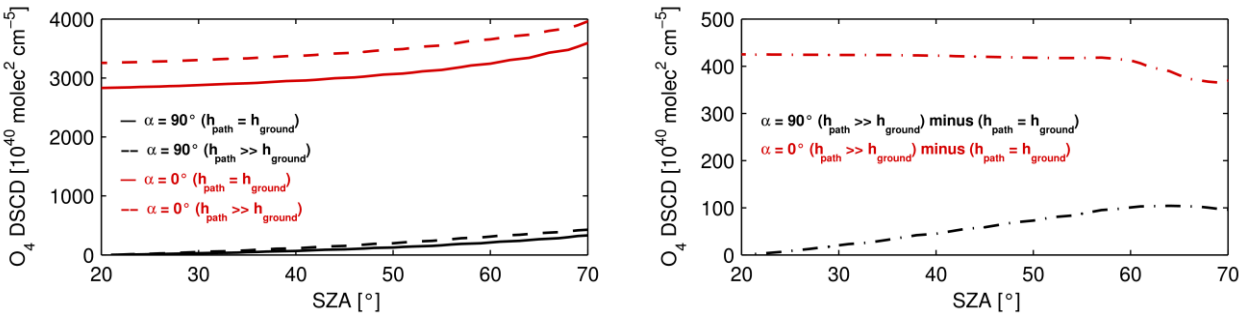

Figure 3. Simulated O_4 DSCDs (346-372 nm fitting window) at the Pico Espejo site (left) for α = 0° (red) and α = 90° (black), where the solid ($h_{path} = h_{ground}$) and dashed ($h_{path} >> h_{ground}$) lines denote the two different scenarios as described in the text and shown in Fig. 1. The absolute differences between the two scenarios are shown in the right panel for the horizontal and vertical viewing direction.

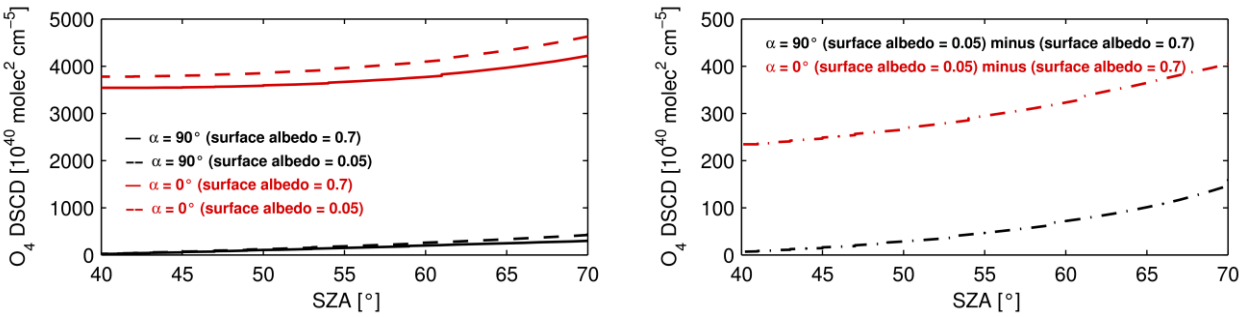

Figure 4. Simulated O_4 DSCDs (346-372 nm fitting window) at the Zugspitze site for $\alpha = 0°$ (red) and $\alpha = 90°$ (black) assuming a surface albedo of 0.05 (solid line) and 0.7 (dashed line). The absolute differences between the two scenarios are shown in the right panel for the horizontal and vertical viewing direction.

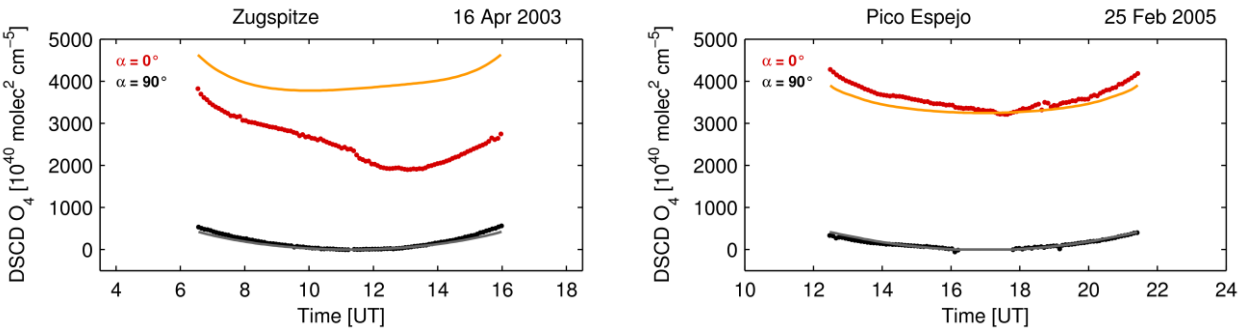

Figure 5. Diurnal evolution of O_4 DSCDs for $\alpha = 0°$ and $\alpha = 90°$ for single days with clear sky conditions at Zugspitze (left) and Pico Espejo (right). Here, O_4 DSCDs are retrieved from measured (red and black lines for $\alpha = 0°$ and $\alpha = 90°$, respectively) and synthetic (orange and gray lines for $\alpha = 0°$ and $\alpha = 90°$, respectively) spectra in the 346-372 nm fitting window and only shown for SZAs < 70° (see Sect. 3).

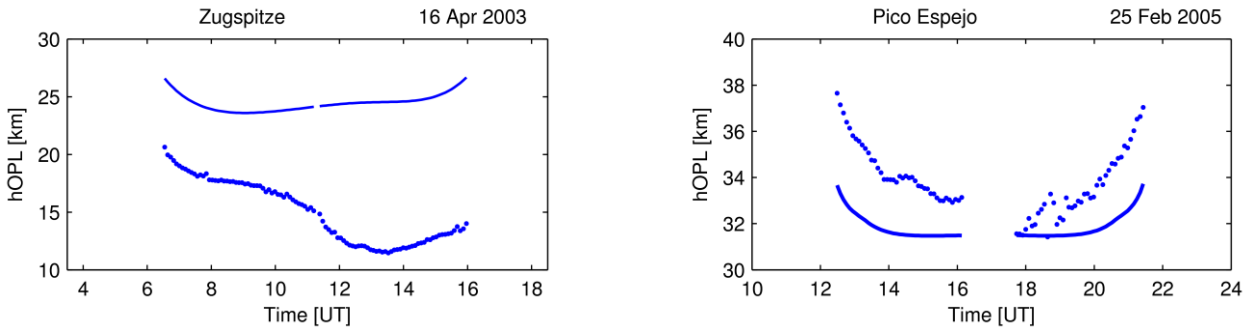

Figure 6. Horizontal optical path length (hOPL) for two single days at Zugspitze (left) and Pico Espejo (right). Here, hOPL is obtained from measured (dotted line) and synthetic (solid line) O_4 DSCDs in the 346-372 nm fitting window and only shown for SZA < 70° (see Sect. 3).

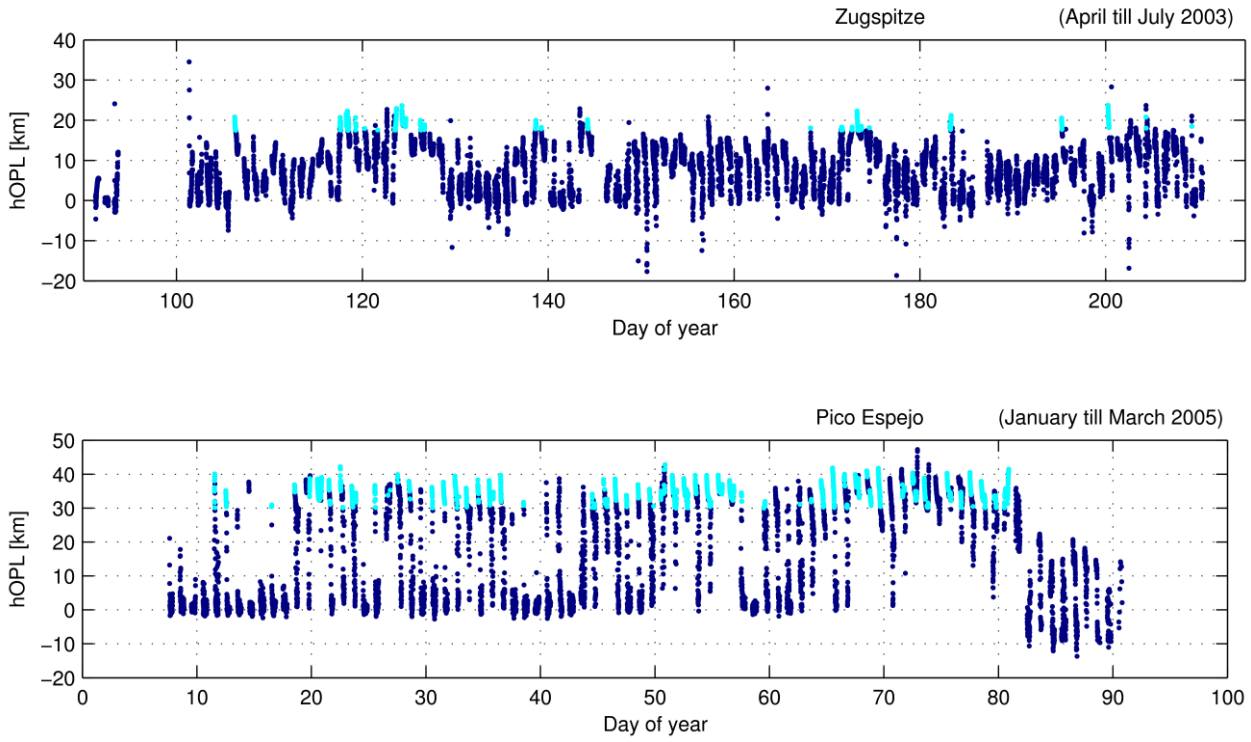

Figure 7. Time series of hOPL before (blue) and after (cyan) applying the filter criteria as defined in Sect. 6.2. Here, hOPL is obtained in the 346-372 nm fitting window and shown for the period April till July 2003 at Zugspitze (upper panel) and for an exemplary dry season (January till March 2005) at Pico Espejo (lower panel).

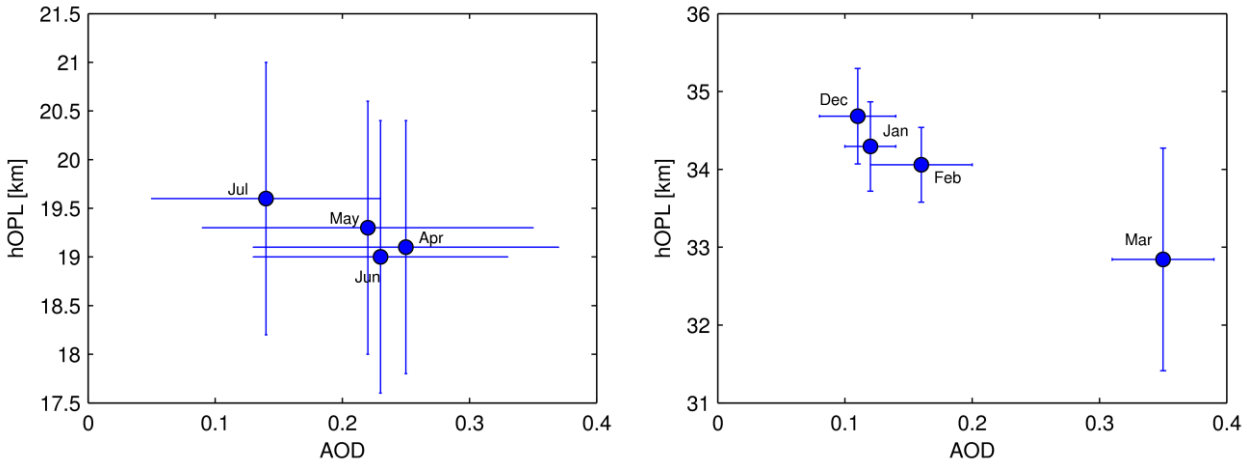

Figure 8. Monthly averaged hOPLs at Zugspitze and multi-year averaged (2004-2009) monthly means of hOPLs at Pico Espejo as a function of spatially averaged aerosol optical depth (AOD) over selected regions (see Table 3). The standard deviation of daily and monthly means is given for Zugspitze and Pico Espejo, respectively (see Table 3). Here, hOPL is obtained from O_4 DSCDs as retrieved for the 346-372 nm fitting window and AOD measurements at 550 nm from MODIS are used.

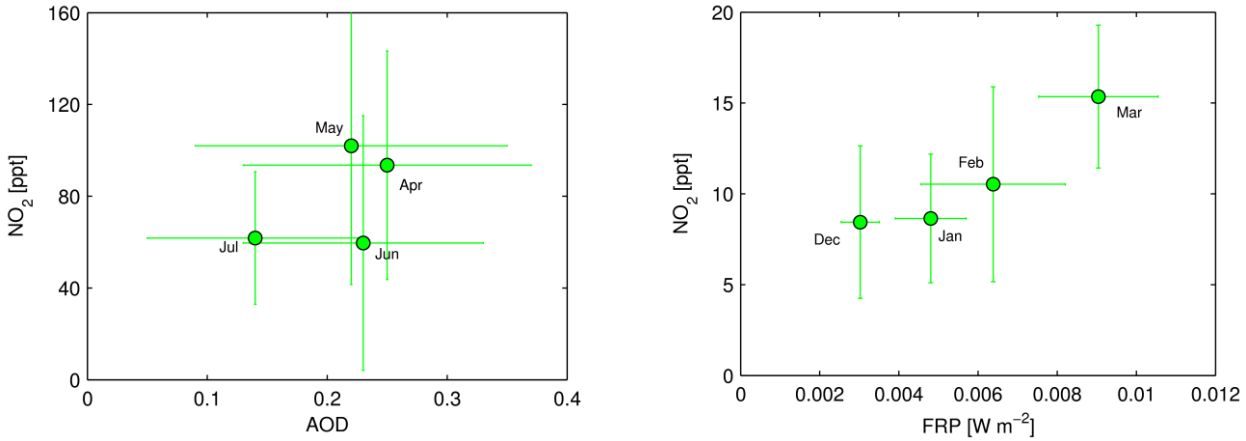

Figure 9. Monthly averaged X_{NO2} at Zugspitze as a function of AOD and multi-year averaged (2004-2009) monthly means of X_{NO2} at Pico Espejo as a function of spatially averaged fire radiative power (FRP) over selected regions (see Table 3). The standard deviation of daily and monthly means is given for Zugspitze and Pico Espejo, respectively (see Table 3).

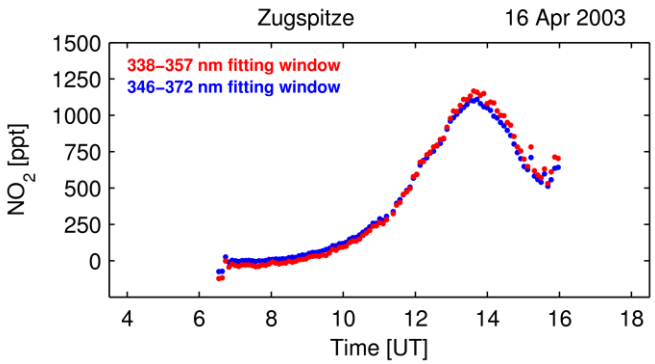

Figure 10. Diurnal evolution of X_{NO2} (for SZA < 70°, but without applying the other filter criteria as described in Sect. 6.2) on 16th April 2003 at Zugspitze as derived using the 338-357 nm (red) and 346-372 nm (blue) fitting windows.

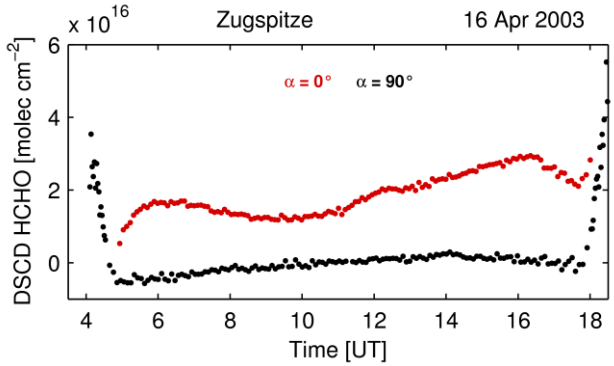

Figure 11. Diurnal evolution of HCHO DSCDs for α = 0° (red) and α = 90° (black) on 16th April 2003 at Zugspitze as retrieved from measured spectra using the 338-357 nm fitting window.

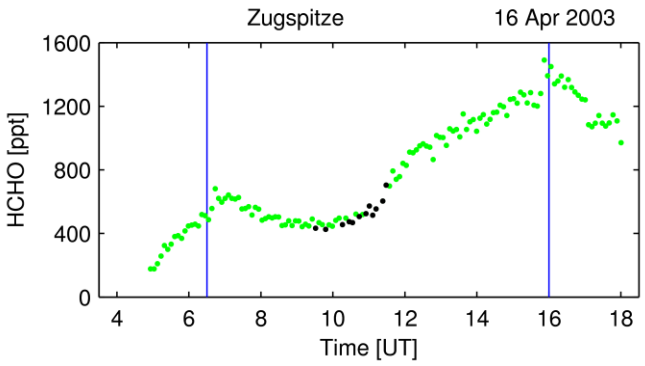

Figure 12. Diurnal evolution of X_{HCHO} on 16th April 2003 at Zugspitze without (green) and with (black) applying the filter criteria as described in Sect. 6.2. The two blue lines indicate SZA = 70° on that day.

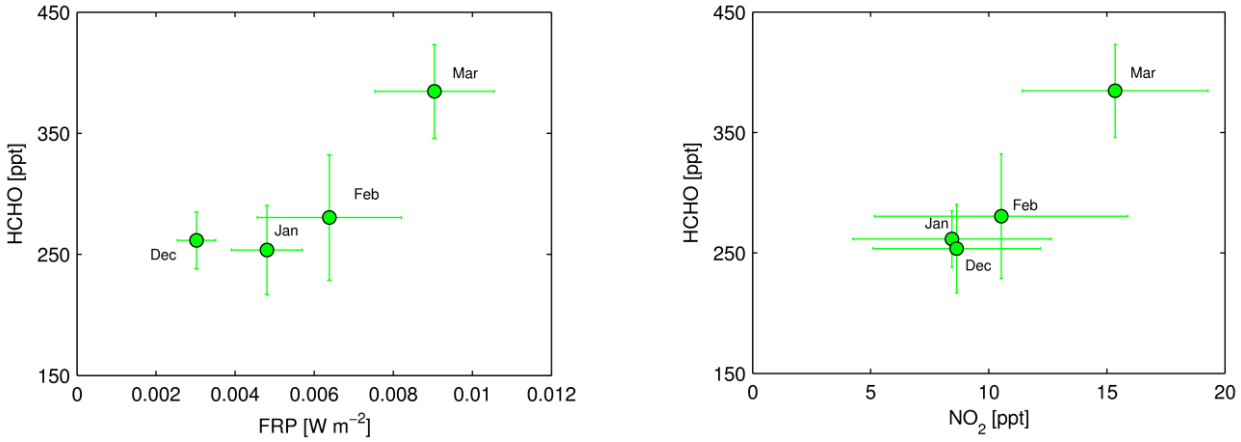

Figure 13. Multi-year averaged (2004-2009) monthly means of X_{HCHO} as a function of spatially averaged FRP over selected regions (see Table 3) (left) and multi-year averaged (2004-2009) monthly means of X_{HCHO} as a function of X_{NO2} (right) at Pico Espejo. The standard deviation of monthly means is given (see Table 3).